Nanostructures

Uniform, Axial-Orientation Alignment of One-Dimensional Single-Crystal Silicon Nanostructure Arrays**

*Kuiqing Peng, Yin Wu, Hui Fang, Xiaoyan Zhong, Ying Xu, and Jing Zhu**

Among the various nanostructures, one-dimensional (1D) single-crystal semiconducting nanostructures are considered to be the most critical building blocks for nanoscale optoelectronics.[1–4] Silicon, the most important semiconducting material in microelectronics, and its 1D nanostructures have attracted attention owing to their potential application in integrated optoelectronic nanodevices.[5–8] To date, various

[*] Dr. K. Peng, Y. Wu, H. Fang, X. Zhong, Y. Xu, Prof. J. Zhu
Department of Materials Sciences and Engineering
Tsinghua University
Beijing, 100084 (China)
Fax: (+86) 10-6277-2507
E-mail: jzhu@mail.tsinghua.edu.cn

Dr. K. Peng
Department of Physics and Materials Science
Center of Super-Diamond and Advanced Films (COSDAF)
City University of Hong Kong
Hong Kong SAR (China)

Y. Xu
Institute of Solar Energy Research
Beijing 100084 (China)

[**] This work was supported by the National Natural Science Foundation, National 973 Project of the People's Republic of China, and 985 Project of Tsinghua University.

Supporting information for this article is available on the WWW under http://www.angewandte.org or from the author.

 DOI: 10.1002/ange.200462995

methods including chemical vapor deposition (CVD),[9] laser ablation,[10,11] and other methods[12,13] have been developed to prepare 1D silicon nanostructures. These syntheses are quite accessible and well-controlled; for example, single-crystal silicon nanowires with controlled diameters have been prepared by using laser-assisted catalytic growth.

The axial crystallographic orientations of 1D silicon nanostructures are expected to influence their electronic structure (energy gap) as well as their physical properties (electron transport) according to previous theory calculations.[14,15] Holmes et al. reported a novel technique that employed supercritical solutions to prepare silicon nanowires with controlled thickness and orientations[13] and found that the wires formed at different pressures exhibited different preferential axial orientations. Their work opened the way to a new area of research: the orientation-controlled synthesis of 1D nanostructures. Accurate control over the axial crystallographic orientations of obtained silicon nanowires remains a challenge, both scientifically and technically. Therefore, to find simpler and quicker ways to produce 1D silicon nanostructures with desirable axial crystallographic orientation is still extremely desirable and of great importance to materials synthesis and future nanoscale optoelectronic devices that employ silicon.

We recently reported a chemical etching method to prepare large-area silicon nanowire arrays.[16,17] However, owing to the strong reaction between silicon and solutions of $HF/AgNO_3$ as well as the large quantities of silver dendrites produced by the galvanic displacement reaction, the exploration and understanding of the reaction mechanism is not easily accessible. Herein, we describe a simple and rapid metal-nanoparticle-assisted etching process to prepare large-area, highly oriented 1D silicon nanostructure arrays on single-crystal silicon wafers. The mechanism for the growth of 1D silicon nanostructures is also readily explored herein owing to the absence of large quantities of silver dendrites. More importantly, our detailed high-resolution electron microscopy (HREM) structural analysis indicates that single-crystal high-quality silicon nanowires (SiNWs) with desirable crystallographic orientation can be readily and controllably created by selecting silicon wafers with a corresponding crystallographic orientation. Optical reflection measurements also demonstrate that the obtained films of 1D silicon nanostructure arrays could suppress the optical reflection drastically over a wide spectral bandwidth. This remarkable characteristic makes it a promising candidate for antireflective surfaces over a large area on silicon wafers.

The production of our 1D silicon nanostructure arrays is quite simple and comprises three steps: 1) cleaning of the silicon wafers with cleaning solution, 2) electroplating the films of metal nanoparticles onto the cleaned silicon surface, and 3) immersion of the nanoparticle-covered silicon wafers into HF-based aqueous chemical etching solutions contained in sealed vessels and treatment for the desired time (at 20 to 60 °C, see Experimental Section). After the preparation process, the obtained samples were rinsed copiously in deionized water and dried at room temperature. The thickness of the films (or length of 1D silicon nanostructures) could be effectively controlled through adjusting the treatment time. The size of the films could be readily made as large as required and is ultimately limited only by the dimensions of the vessel.

Characterization of our as-synthesized samples by scanning electron microscopy (SEM) confirms that large-area highly oriented 1D silicon nanostructure arrays can be created on single-crystal silicon wafers around room temperature. Figure 1 shows the transmission electron microscopy

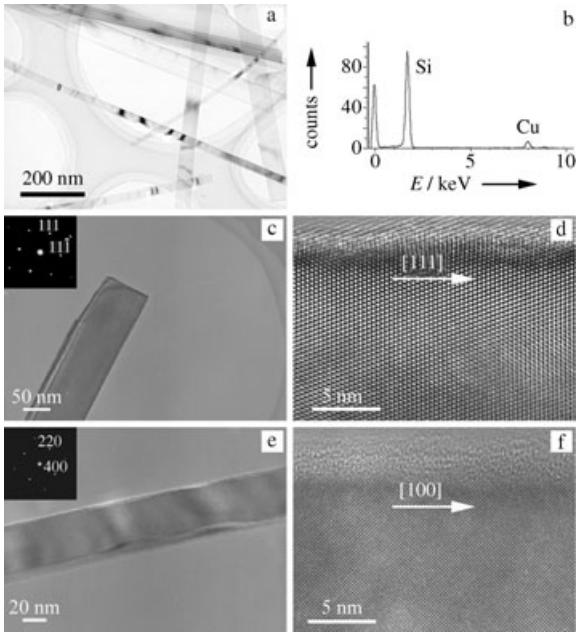

Figure 1. TEM images of as-synthesized 1D silicon nanostructures. a) Several nanowires and nanoribbons, b) an EDX spectrum recorded from one nanowire, c) an individual silicon nanoribbon synthesized from a p-type [111] silicon wafer (the inset shows its ED pattern recorded along the [$\bar{1}$10] axis), d) HREM image of the section of nanoribbon shown in part (c), e) an individual silicon nanowire synthesized from a p-type [100] silicon wafer, (the inset shows its ED pattern recorded along the [001] axis), and f) HREM image of the section of the nanowire shown in part (e).

(TEM) images of as-synthesized samples, which were prepared by deposition of a film of silver nanoparticles onto a silicon surface from a solution of $HF/AgNO_3$, followed by immersion of the treated silicon substrate into an aqueous solution of $HF/Fe(NO_3)_3$ at 50 °C for 30 minutes. 1D wire- and ribbonlike nanostructures can be clearly seen in Figure 1a. The electron diffraction (ED) patterns recorded from these 1D nanostructures show their single-crystal characteristics. Figure 1b is a representative energy-dispersive X-ray (EDX) spectrum for a nanoribbon sample and shows only a peak for silicon (the signal for copper originates from the supporting copper grid). Figure 1c is a TEM image of an individual nanoribbon prepared from a p-type silicon wafer with [111] orientation, and the inset is an ED pattern recorded from the nanoribbon, which could be indexed as the [$\bar{1}$10] zone axis of single-crystal silicon. Figure 1d shows the HREM image of the section of nanoribbon shown in Figure 1c. Analysis by ED and HREM indicate that the axial orientation of the nanoribbon is the [111] direction,

which is the same as that of the initial silicon wafer. Figure 1e and f show the TEM images and ED pattern recorded from a nanowire prepared from a p-type silicon wafer with [100] orientation. Analysis of these TEM images clearly indicates that the nanowire grows along the [100] direction, which is identical to the orientation of the initial silicon wafer.

Further experiments confirmed that the axial crystallographic directions of as-synthesized 1D silicon nanostructures are determined by the orientation of the initial silicon wafers used. More specifically, 1D silicon nanostructures with desirable orientations could be created through selecting silicon wafers with identical orientations. Furthermore, the p- and n-type silicon wafers used in our experiments show near-identical behavior, thus 1D silicon nanostructures with desirable conduction type could also be readily obtained. Generally, etching generates regular or irregular etching pits. Here, however, it is surprising to see that the etched nanostructures are smooth and there is almost no diameter modulation along the long nanostructure axis for both types of wires. These results imply that smooth nanostructures may result from the special metal-nanoparticle catalytic etching process.

We named the as-synthesized samples "black silicon" owing to their black color, which also implies their potentially high antireflection property. Figure 2 shows a comparison of the hemispherical reflectance of 1D silicon nanostructure arrays and a polished silicon wafer. The reflectance of the films is drastically decreased relative to that of the polished silicon wafer over a broad spectral range (samples 1 and 2 are silver-treated silicon wafers treated in a solution of HF/$Fe(NO_3)_3$ for 50 and 30 min, respectively). The reflectance of the 1D silicon nanostructure films is less than 1.46% over the range 300–600 nm. This remarkable property suggests films of 1D silicon nanostructure arrays as candidates of antireflective surfaces. The ultralow reflectance of the 1D silicon nanostructure films may be a result of the high density of 1D silicon nanostructures and also the subwavelength-structured (SWS) surface, which could suppress reflection over a wide spectral bandwidth and a large field of view.[18]

The generally accepted growth mechanism of 1D silicon nanostructures is the vapor–liquid–solid (VLS) growth mechanism,[9,10] which is based on growth from a liquid metal seed particle. We suggest that the formation mechanism of the as-synthesized 1D silicon nanostructures is quite different from previously proposed mechanisms.[9,11,13,16,19] To clarify the formation mechanism of the 1D silicon nanostructures, detailed investigations were carried out on the silver-nanoparticle-assisted catalytic etching of silicon in a solution of HF/$Fe(NO_3)_3$.

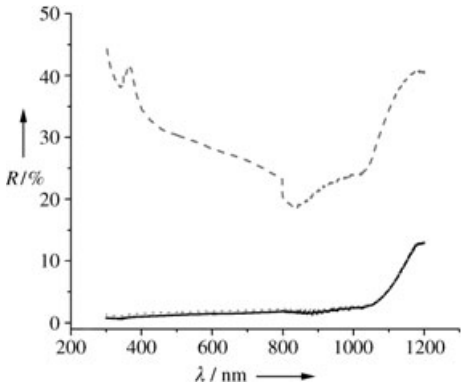

Figure 2. Reflectance (R) as a function of wavelength. Samples 1 (——) and 2 (----) were prepared by treating a silver-covered silicon wafer in an aqueous solution of HF/$Fe(NO_3)_3$ for 50 and 30 minutes, respectively. (Polished silicon: – – –).

Networks of silver nanoparticles were produced on silicon surfaces by the galvanic displacement reaction on treatment of the silicon wafer in a solution of HF/$AgNO_3$ for one minute (Figure 3a). Figure 3b–f show the morphological evolution process of a p-type [111] silicon wafer in HF/$Fe(NO_3)_3$ solution. With the elapse of treatment time, silver nanoparticle networks gradually sank into the bulk silicon and 1D silicon nanostructure arrays gradually emerged. Large-area oriented high-aspect-ratio 1D silicon nanostructure arrays could be produced on the silicon surface after immersion for 50 minutes in HF/$Fe(NO_3)_3$ solution (Figure 3f). This sinking behavior of silver nanoparticles could be seen clearly through

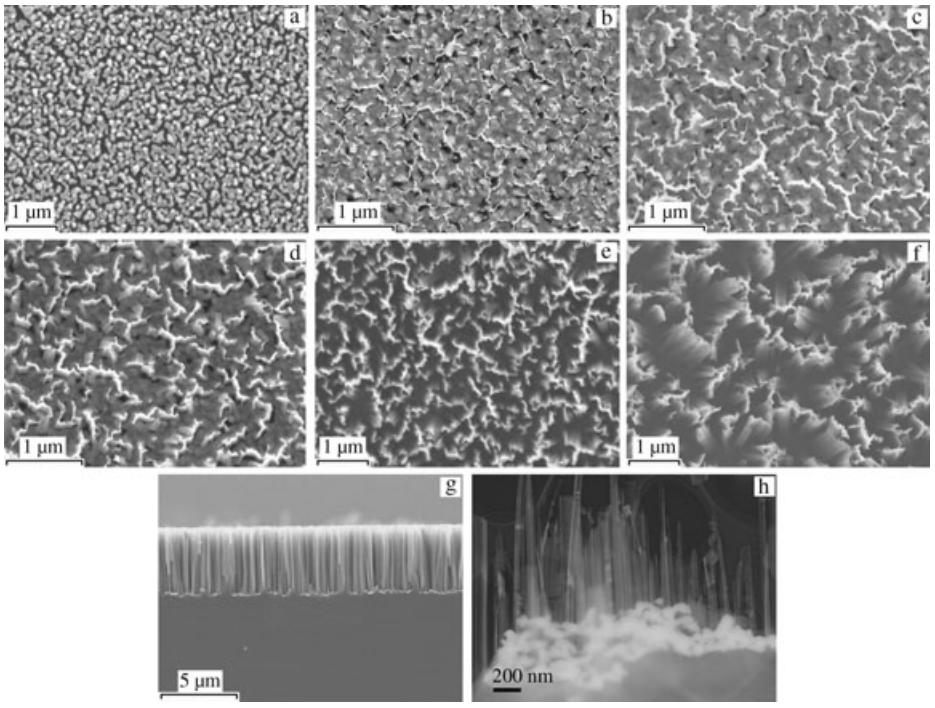

Figure 3. a–f) SEM images showing the morphological evolution of a silicon wafer in HF/$Fe(NO_3)_3$ solution at a) $t=0$, b) $t=2$, c) $t=5$, d) $t=10$, e) $t=20$, and f) $t=50$ min. g) SEM cross-section image and h) TEM image of the as-synthesized sample (silver nanoparticles can be clearly seen at the interface between the silicon substrate and the film of the 1D silicon nanostructure formed).

an SEM cross-section image (Figure 3 g). Many silver nanoparticles can be seen at the interface between the silicon substrate and the formed film of 1D silicon nanostructures. A TEM image (Figure 3 h) more clearly shows the sunken silver nanoparticles situated at the interface between the silicon substrate and the formed 1D silicon nanostructure array.

These results imply that the collective sinking behavior of silver nanoparticle networks plays an important role in the formation of 1D silicon nanostructure arrays. Therefore, we propose a mechanism that accounts for the formation of 1D silicon nanostructures based on silicon etching and metal deposition electrochemistry in HF-based solution.[20–28] The mechanism of electroless silver deposition on silicon and silver-nanoparticle-catalyzed chemical etching process of silicon in $HF/Fe(NO_3)_3$ solution is shown in Figure 4.

Buriak and co-workers discovered that films of noble-metal nanoparticles could be deposited on germanium by the galvanic displacement reaction in the absence of toxic HF.[27] They suggested that the mechanism for the galvanic displacement reaction on germanium with gold, palladium, and platinum salts with highly positive equilibrium reduction potentials is expected to occur through hole injection into the valence band. They suggested that germanium–germanium bonds could supply the electrons used to reduce the metal salts on the surface, which leads to subsequent dissolution of the germanium substrate as the oxide. However, it remains to be determined if the oxidation and dissolution of the substrate occurs from beneath the metal deposits or alongside them.

In our experimental system, a similar electroless-deposition/semiconductor-etching process as that reported by Buriak for germanium occurs in the case of silicon, except that an etchant such as HF is necessary here because the silicon oxide produced must be etched away and dissolved into water. For the initial electroless deposition of silver from $HF/AgNO_3$ solution on silicon, simultaneous electrochemical processes including cathodic (silver-deposition reaction) and anodic reactions (silicon oxidation and dissolution) occur on the silicon surface. First, Ag^+ ions in the vicinity of the silicon surface capture electrons from the valence band (VB) of silicon and are deposited in the form of metallic silver nuclei (see Supporting Information). With the deposition and growth of silver nuclei, SiO_2 is formed simultaneously underneath the silver nanoparticles (Figure 4a,b). As the SiO_2 underneath the silver nanoparticles is etched away as SiF_6^{2-} by HF, then pits form immediately at the same positions (Figure 4c), so the silver nanoparticles sink into the pits as they form. This is consistent with our SEM observations, which confirmed that the oxidation and dissolution of the silicon substrate occurs from beneath the metal deposits.

In the solution of $HF/Fe(NO_3)_3$, the redox level of the Fe^{3+}/Fe^{2+} system lies well below the VB of silicon, so active kinetics are expected for the electron-capture process from the VB bonding electrons. However, contrary to fast reduction of Ag^+ ions, reduction of Fe^{3+} ions and oxidation of silicon proceed very slowly on the silicon surface in the absence of silver nanoparticles. When the silicon surface is covered with silver nanoparticles, reduction of Fe^{3+} ions and

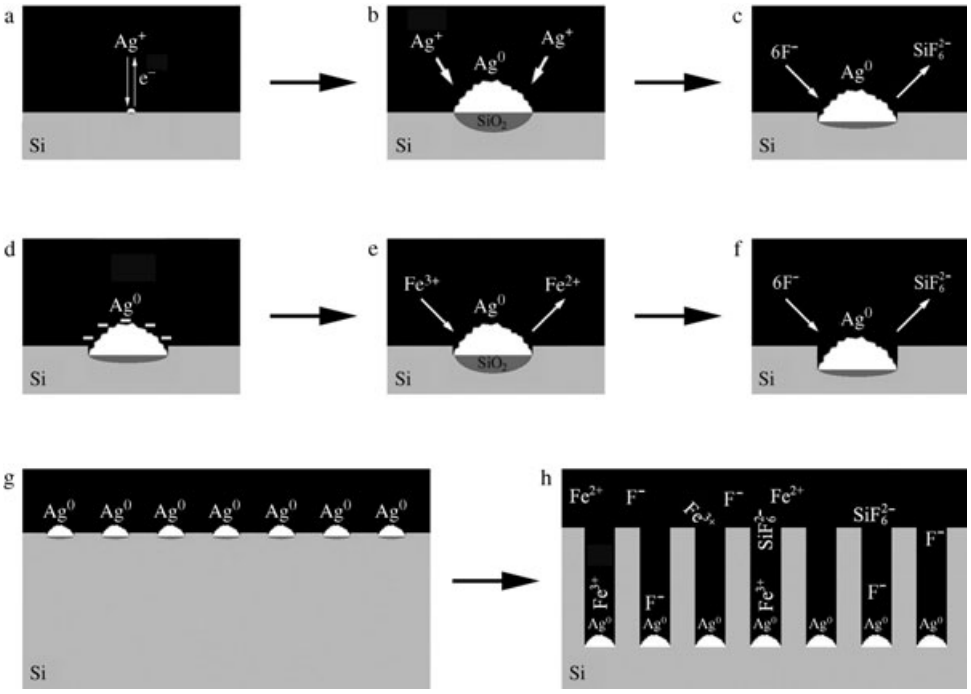

Figure 4. A model illustrating the electroless deposition of silver on silicon in $HF/AgNO_3$ solution and the silver-nanoparticle-catalyzed chemical etching of silicon in $HF/Fe(NO_3)_3$ solution. a–c) Nucleation and growth of silver nanoparticles on the silicon surface in $HF/AgNO_3$ solution: SiO_2 forms simultaneously underneath the silver nanoparticles, and pits form as a result of etching away of SiO_2 in HF solution. d–f) Reduction of Fe^{3+} ions, etching of silicon, and sinking of silver nanoparticles in $HF/Fe(NO_3)_3$ solution: deeper pits are created by the silver nanoparticles. g) Silver nanoparticle arrays form on the silicon surface. h) Deep pores form in the bulk silicon in $HF/Fe(NO_3)_3$ solution as a result of the continuous etching away of SiO_2 underneath the silver nanoparticles.

oxidation of silicon is greatly enhanced. It is generally believed that metal nanoparticles adhered on a silicon surface have a higher electronegativity than silicon, so they could attract electrons from silicon to become negatively charged. These metal nanoparticles could then act as local microcathodes and enhance the cathodic reaction as a result of their catalytic activity.[24,26] Therefore, Fe^{3+} ions have the strong tendency to preferentially obtain electrons from silver nanoparticles and be reduced to Fe^{2+} ions, while the silicon underneath the silver nanoparticles is oxidized to SiO_2. The Ag^+/Ag system has a more positive redox potential than that of the Fe^{3+}/Fe^{2+} couple, so silver nanoparticles are stable and can continue to enhance the reduction of Fe^{3+} ions and the oxidation of silicon in the $HF/Fe(NO_3)_3$ solution. As the silver nanoparticles are pinned by the pits and cannot move horizontally on the silicon surface, selective etching occurs and deeper pits or pores finally form.

According to the above discussion, we suggest that initial shallow pits in silicon could be developed into deeper pores owing to the continuous etching away of SiO_2 and further sinking of silver nanoparticles upon prolonged immersion in the $HF/Fe(NO_3)_3$ solution (Figure 4d). The pores are simply the sinking tracks of silver nanoparticles. For spatially dispersive metal nanoparticles, separated deep pores should form. However, deposited silver nanoparticles have a strong tendency to form interconnected networks under the present silver-deposition conditions adopted. It can be easily understood that the collective sinking behavior of silver networks will cut the bulk silicon into freestanding 1D silicon nanostructures. We suggest that ordered pore arrays could be created if the silicon surface is patterned with ordered active metal-nanoparticle arrays.

Besides demonstrating the silver-nanoparticle-assisted formation of 1D silicon nanostructure arrays on silicon surfaces in $HF/Fe(NO_3)_3$ solution, we also investigated other noble-metal nanoparticles (Cu, Au, and Pt) deposited on silicon. The reduction of Fe^{3+} ions and oxidation of silicon could be greatly enhanced owing to the presence of these metal nanoparticles. However, only shallow pits were formed on the silicon surface for copper as a result of its high solubility, which is caused by its much lower redox potential relative to that of Fe^{3+}/Fe^{2+} in $HF/Fe(NO_3)_3$ solution. $AuCl_4^-/Au$ and $PtCl_6^{2-}/Pt$ have more-positive redox potentials than that for Fe^{3+}/Fe^{2+} (see Supporting Information), so gold and platinum nanoparticles are stable in the solution of $HF/Fe(NO_3)_3$. Gold nanoparticles have a strong tendency to form dense networks under our adopted deposition conditions. Oriented 1D silicon nanostructure arrays formed when gold-covered silicon wafers were treated in the $HF/Fe(NO_3)_3$ solution. In contrast, in the case of platinum, spatially dispersive nanoparticles formed on the silicon surface under these deposition conditions, but no nanoparticle networks were formed. According to our proposed mechanism, only separated deep pores could be created in bulk silicon, and the experimental results justify our model (see Supporting Information).

In conclusion, we have developed a facile metal-nanoparticle-assisted catalytic etching technique to produce large-area highly oriented 1D silicon nanostructure arrays with desirable axial crystallographic orientation. Exact control of the axial crystallographic orientation of 1D silicon nanostructures represents one significant step towards future nanoscale optoelectronic devices that employ silicon. The remarkable antireflection property of the 1D silicon nanostructure films also indicates its potential applicability as an antireflective surface for photovoltaic devices and optical detectors. A reasonable mechanism has been proposed on the basis of convincing experimental evidence. On the basis of our proposed mechanism, we believe that the metal-nanoparticle-assisted catalytic etching technique may also be extended to other materials, such as SiC and GaN.

Experimental Section

Preparation of nanostructure arrays: The synthesis of large-area oriented 1D silicon nanostructure arrays was conducted in a teflon-lined stainless steel autoclave. The production process comprised three steps: 1) cleaning the silicon wafers with cleaning solution—here we sequentially used acetone (5 min), ethanol (5 min), deionized water (2–3 times), and H_2SO_4/H_2O_2 (3:1 H_2SO_4 (97%)/H_2O_2 (30%), 10 min), then the wafers were thoroughly rinsed with deionized water (10 min) and dipped into a solution of HF (1 min); 2) electroplating the metal-nanoparticle films onto the cleaned silicon surface; and 3) immersion of the metal-nanoparticle-covered silicon wafers into HF-based aqueous chemical etching solutions contained in a sealed vessel and treated for the desired time (20–60 °C). After the preparation process, the obtained samples were rinsed copiously in deionized water and dried at room temperature.

All the experiments described here were performed at 50 °C. The thickness of films (or the length of 1D silicon nanostructures) could be effectively controlled through adjusting the etching time, and film sizes could be readily made as large as needed and are ultimately limited only by the vessel dimensions. The deposition of various metals and their influence on the etching morphologies of silicon were investigated. The concentrations of HF and $AgNO_3$ for the deposition of Ag nanoparticle films were 4.6 and 0.01 M, respectively, while the concentrations of HF and $Fe(NO_3)_3$ for etching the silver-nanoparticle-covered silicon wafers were 4.6 and 0.135 M, respectively.

Characterization: After preparation, the samples were studied by SEM (JEOL 6301F) and TEM (JEOL 2010F) equipped with an energy-dispersive X-ray spectrometer and a Gatan GIF 678 system. The samples for TEM were prepared by scraping the bulk sample with a knife, and then the scraping was collected and suspended in ethanol. A drop of this suspension was then placed on a carbon–copper grid and examined under a JEOL 2010F microscope. Optical reflectance measurements were performed with a Hitachi U-4001 UV/Vis spectrophotometer.

Received: December 20, 2004
Published online: April 6, 2005

Keywords: electrochemistry · nanostructures · semiconductors · silicon

[1] M. Law, J. Goldberger, P. D. Yang, *Annu. Rev. Mater. Res.* **2004**, *34*, 83.
[2] M. Law, D. J. Sirbuly, J. C. Johnson, J. Goldberger, R. J. Saykally, P. D. Yang, *Science* **2004**, *305*, 1269.
[3] X. F. Duan, Y. Huang, R. Agarwal, C. M. Lieber, *Nature* **2003**, *421*, 241.
[4] X. F. Duan, Y. Huang, Y. Cui, J. F. Wang, C. M. Lieber, *Nature* **2001**, *409*, 66.

[5] X. Y. Zhao, C. M. Wei, L. Yang, M. Y. Chou, *Phys. Rev. Lett.* **2004**, *92*, 236805.
[6] D. D. D. Ma, C. S. Lee, F. C. K. Au, S. Y. Tong, S. T. Lee, *Science* **2003**, *299*, 1874.
[7] D. Y. Li, Y. Y. Wu, P. Kim, L. Shi, P. D. Yang, *Appl. Phys. Lett.* **2003**, *83*, 2934.
[8] Y. Cui, C. M. Lieber, *Science* **2001**, *291*, 851.
[9] J. Westwater, D. P. Gosain, S. Tomiya, S. Usui, H. Ruda, *J. Vac. Sci. Technol. B* **1997**, *15*, 554.
[10] A. M. Morales, C. M. Lieber, *Science* **1998**, *279*, 208.
[11] N. Wang, Y. F. Zhang, Y. H. Tang, C. S. Lee, S. T. Lee, *Appl. Phys. Lett.* **1998**, *73*, 3902.
[12] D. P. Yu, Z. G. Bai, Y. Ding, Q. L. Hang, H. Z. Zhang, J. J. Wang, Y. H. Zou, W. Qian, G. C. Xiong, H. T. Zhou, S. Q. Feng, *Appl. Phys. Lett.* **1998**, *72*, 3458.
[13] J. D. Holmes, K. P. Johnston, R. C. Doty, B. A. Korgel, *Science* **2000**, *287*, 1471.
[14] C. Delerue, G. Allan, M. Lannoo, *Phys. Rev. B* **1993**, *48*, 11024.
[15] H. Yorikawa, H. Uchida, S. Muramatsu, *J. Appl. Phys.* **1996**, *79*, 3619.
[16] K. Q. Peng, Y. J. Yan, S. P. Gao, J. Zhu, *Adv. Mater.* **2002**, *14*, 1164.
[17] K. Q. Peng, Z. P. Huang, J. Zhu, *Adv. Mater.* **2004**, *16*, 73.
[18] Y. Kanamori, M. Sasaki, K. Hane, *Opt. Lett.* **1999**, *24*, 1422.
[19] K. Q. Peng, Y. J. Yan, S. P. Gao, J. Zhu, *Adv. Funct. Mater.* **2003**, *13*, 127.
[20] N. Mitsugi, K. Nagai, *J. Electrochem. Soc.* **2004**, *151*, G302.
[21] P. Gorostiza, P. Allongue, R. Diaz, J. R. Morante, F. Sanz, *J. Phys. Chem. B* **2003**, *107*, 6454.
[22] L. Magagnin, R. Maboudian, C. Carraro, *J. Phys. Chem. B* **2002**, *106*, 401.
[23] J. S. Kim, H. Morita, J. D. Joo, T. Ohmi, *J. Electrochem. Soc.* **1997**, *144*, 3275.
[24] P. Gorostiza, R. Diaz, J. Servat, F. Sanz, J. R. Morante, *J. Electrochem. Soc.* **1997**, *144*, 909.
[25] G. J. Norga, M. Platero, K. A. Black, A. J. Reddy, J. Michel, L. C. Kimerling, *J. Electrochem. Soc.* **1997**, *144*, 2801.
[26] L. Teerlinck, P. W. Mertens, H. F. Schmidt, M. Meuris, M. M. Heyns, *J. Electrochem. Soc.* **1996**, *143*, 3323.
[27] L. A. Porter, H. C. Choi, A. E. Ribbe, J. M. Buriak, *Nano Lett.* **2002**, *2*, 1067.
[28] H. Morinaga, M. Suyama, T. Ohmi, *J. Electrochem. Soc.* **1994**, *141*, 2834.

